Vacuum 214 (2023) 112248

Contents lists available at ScienceDirect

Vacuum

journal homepage: www.elsevier.com/locate/vacuum

Morphology and structure of $CdCl_2$-Containing CdTe films deposited by discrete vacuum thermal evaporation

V.A. Gevorgyan [a,**], N.R. Mangasaryan [a], V.F. Gremenok [b], M.S. Tivanov [c], Preeti Thakur [d,e], Atul Thakur [d,e], S.V. Trukhanov [b], T.I. Zubar [b], M.I. Sayyed [f,g], D.I. Tishkevich [b,*], A. V. Trukhanov [b,h]

[a] Russian-Armenian (Slavonic) University, Physico-Engineering Institute Department of Materials Technology and Structure of Electronic Technique, 0051, Yerevan, Armenia
[b] Laboratory of Magnetic Film Physics, Scientific-Practical Materials Research Centre of NAS of Belarus, 220072, Minsk, Belarus
[c] Belarusian State University, Faculty of Physics, Nezavisimosti 4 Av., 220030, Minsk, Belarus
[d] Centre of Nanotechnology, Amity University Haryana, Gurugram, 122413, Haryana, India
[e] NanoLatticeX, Amity University Haryana, Gurugram, 122413, Haryana, India
[f] Department of Physics, Faculty of Science, Isra University, 1162, Amman, Jordan
[g] Department of Nuclear Medicine Research, Institute for Research and Medical Consultations (IRMC), Imam Abdulrahman Bin Faisal University, Dammam, 31441, Saudi Arabia
[h] L.N. Gumilyov Eurasian National University, 010000, Nur-Sultan, Kazakhstan

ARTICLE INFO

Handling Editor: Prof. L.G. Hultman

Keywords:
Discrete vacuum thermal evaporation
Cadmium telluride (CdTe)
$CdCl_2$ treatment
Thin film
Solar cells

ABSTRACT

The impact of discrete vacuum thermal evaporation (DVTE)-produced CdTe thin films after thermal annealing and $CdCl_2$ treatment is discussed in the present article. As a result of simultaneous DVTE of $CdCl_2$ and CdTe, $CdCl_2$ was added straightly into the bulk of the formed CdTe film at the 270 °C substrate temperature in a single procedure. The DVTE approach deposits CdTe thin films with a high crystalline structure, which can be utilized effectively for the production of high efficiency solar cell applications, according to the results of X-ray diffraction, scanning electron microscopy with focused ion beam, transmission electron microscopy, and atomic force microscopy measurements.

1. Introduction

Sunlight is the most abundant source of energy on earth. The conversion of sunlight energy into electricity offers tremendous opportunities for reducing the carbon footprint of fossil-fuel-based energy technologies on the global environment. Cadmium telluride (CdTe) is a direct-bandgap material with ~1.5 eV bandgap energy at room temperature [1–6]. It is an optimal material for converting solar light energy into electricity due to its high (above 5×10^4 cm^{-1}) visible spectrum coefficient of absorption [2,7–11]. Thin-film CdTe-based solar cells represent ~5% of the present world market for photovoltaic technology [12]. The manufacturing method for these cells is relatively affordable [4,5,12,13]. It provides a lower-cost alternative to silicon-based solar technologies [14,15]. The highest light conversion efficiency in laboratory settings for CdTe cells is 22.1% [12]. The aver-age efficiency for commercial modules is ~17% [12]. CdTe-based solar cells exhibit superior radiation damage tolerance, which makes them ideal candidates for space photovoltaic applications [16,17].

The current manufacturing technology of these cells uses the closed-space sublimation (CSS) method for CdTe thin-film deposition [18–23]. CSS is an energy-intensive process with a high temperature (650–700 °C) deposition stage, requiring the use of heat-resistant, rigid glass substrates. Unlike glass substrates, the deposition of CdTe on lightweight polymers is impossible due to the high evaporation temperatures of the CSS process. Such polymer substrates could decrease the total weight of CdTe solar cells by more than 90%. This weight reduction will make them better suited for space, low-power devices, electric vehicles, drones, and other emerging applications. Therefore, it is crucial to reduce the deposition temperature for CdTe films. The reported approaches for CdTe film fabrication include pulsed laser deposition [7,

* Corresponding author.
** Corresponding author.
E-mail addresses: vladimir.gevorgyan@rau.am (V.A. Gevorgyan), dashachushkova@gmail.com (D.I. Tishkevich).

https://doi.org/10.1016/j.vacuum.2023.112248
Received 21 May 2023; Received in revised form 29 May 2023; Accepted 30 May 2023
Available online 31 May 2023

24], electrodeposition [25,26], molecular beam epitaxy [10,27], chemical vapor deposition [11,28], magnetron sputtering [29,30] and thermal vacuum evaporation [31–39].

The sputtering and evaporation methods demonstrate a higher potential to develop low-temperature deposition procedures for CdTe films. Magnetron sputtering provides high-quality materials, but it utilizes expensive and specially manufactured source materials (targets). The use of thermal vacuum evaporation offers high control over the deposition process and the ability to automate manufacturing of large-area solar cells. However, conventional evaporation produces crystallographically defective films for complex semiconductors due to the difference in partial pressures of source material components (as is distinguishable for II-VI semiconductor chalcogenide compounds, for instance).

A thermally evaporated thin layer of $CdCl_2$ on CdTe often helps to improve the efficiency of CdTe-based solar cells [40–45]. Another method for improving film quality is to dip CdTe films in a $CdCl_2$-containing solution after deposition, followed by an annealing step (350–400 °C) in the air [46–48]. The diffusion of $CdCl_2$ into the CdTe layer creates CdO upon oxidation, which passivates the CdTe grains. Meanwhile, the annealing reduces the defects in the crystal structure.

Discrete vacuum thermal evaporation (DVTE), also known as flash evaporation, overcomes the disadvantages of conventional evaporation for the chalcogenide film deposition process [49–52]. This method utilizes a controlled supply of chalcogenide source materials in the pre-heated evaporation boats. As a result of this, the boat contains particles at different evaporation stages and temperatures at any given time. This fact, in turn, ensures a constant atomic flux of vaporizing components to maintain the desired stoichiometry of constituents in the deposited layer.

In our previous works, we used this method to grow high-quality CdS and CdTe films with the same bandgap energy as the corresponding bulk materials [51,52]. Atomic force microscopy (AFM) imaging and X-ray diffraction (XRD) patterns demonstrate that these films have excellent morphological uniformity and low crystalline defects [52].

In this work, we report an in situ DVTE deposition procedure for $CdCl_2$-containing CdTe film preparation at a substrate temperature of 270 °C and an evaporator temperature of 600 °C–650 °C. Here, we present links between processing conditions, including post-deposition annealing, morphology, and the structure of thin films as a function of the $CdCl_2$ content in the deposited films. This deposition technique could pave the way for preparing high-quality CdTe films on lightweight substrates.

2. Experimental procedures

CdTe thin films were deposited using the DVTE method on ordinary glass substrates with a thickness of 1 mm and a diameter of 20 mm. Before the deposition, the glass pieces underwent cleaning using an ultrasonic bath with a surfactant solution and then a rinse with distilled water to remove any remaining surfactant. Then, the substrates were rewashed with high purity methanol using an ultrasonic bath.

To make a source material powder, a single-crystal CdTe with a purity of 99.999% (Sigma-Aldrich, USA) was crushed and ground. The powder was sieved to obtain particles with a size of 100–150 μm, which were placed inside a vertically positioned vessel. Fig. 1 shows a schematic representation of the evaporator used to deposit CdTe films. CdTe powder (marked with 1) is placed inside the vessel (2) and fed into the molybdenum-made evaporation boat (3) by an automatically controlled vibrating outlet (4). The opening duration (0.2–0.5 s) of the outlet controls the CdTe supply speed to the boat. The deposition of films was conducted at a base pressure of $\sim 2 \times 10^{-3}$ Pa. The temperature of the evaporating boat was kept at 600–650 °C, while the substrate (5) temperature was maintained at 270 °C using a thermocouple-controlled heater (6). The distance between the boat and the substrate was ~12 cm. The deposition durations varied between 30 and 60 min to obtain

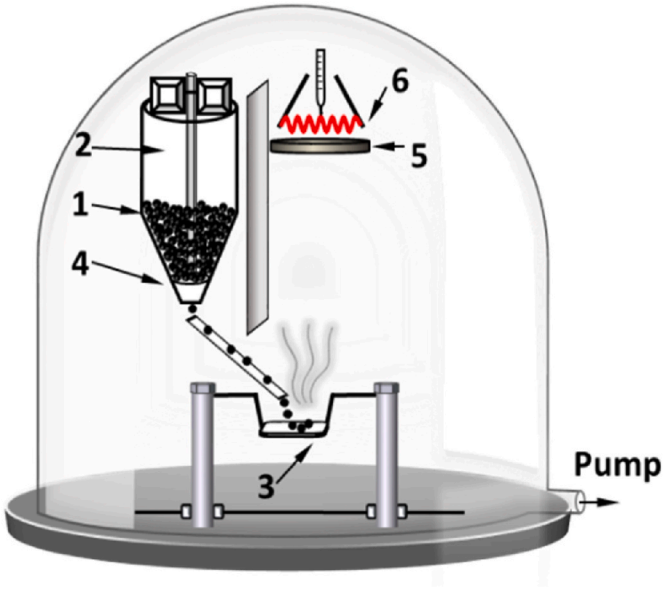

Fig. 1. Schematics of the evaporator setup: CdTe powder (1), vessel (2), Mo evaporation boat (3), vibrating vessel outlet (4), substrate (5), thermocouple-controlled heater (6).

films with a thickness of 2–4 μm.

Three samples, denoted as sample A, B, and C, were subjected to deposition. Sample A was produced by evaporating pure CdTe. The preparatory work of samples B and C involved the synchronous evaporation of CdTe and $CdCl_2$ with atomic fractions of $\frac{N_{CdCl_2}}{N_{CdTe}} = 10^{-4}$ and $\frac{N_{CdCl_2}}{N_{CdTe}} = 10^{-3}$, respectively. In the air (20% oxygen), samples underwent post-deposition thermal annealing for 60 min at 350 °C. Samples that have been annealed were marked as A*, B*, and C*, respectively.

The CdTe film structure was investigated by an X-ray diffractometer (URD-6) in the θ-2θ operating regime using CuKα (λ = 0.15405 nm) radiation in the range 10°-100° with a step of 0.01°. With the help of AFM (NEXT, NT-MDT Inc.), the surface morphology and roughness of CdTe films were studied. The microstructures of samples were also examined with a scanning electron microscope (SEM, Magellan 400, FEI). For producing of cross-sections on thin films by gallium ion beam milling a Helios NanoLab600 system (FEI) with a dual-beam microscope was used [53,54]. First, platinum layer with a 0.3 μm thick and 10 μm × 0.5 μm rectangular area was deposited onto the selected material area. Then, 5–10 μm deep trench with a 45° base angle was milled on the surface with milling current of 27 nA and under an accelerating voltage of 5 keV. A layer of 5 μm thick was milled in the sidewall of the trench with milling current of 700 pA under an accelerating voltage of 5 keV for producing a qualitative cross-section without any artifacts. To image the sidewall of the trench the electron-beam was applied. Dark field and high-resolution transmission electron microscope (TEM) imaging of samples along with electron diffraction analysis were performed with a Titan 80–300 (FEI) microscope at 300 keV. The TEM samples were prepared using a Helios NanoLab 600 system by making thin (~50–70 nm) cross-sectional slices.

3. Results and discussion

3.1. The crystalline structure of films

Fig. 2 shows XRD patterns for as-deposited and annealed CdTe thin films. As-deposited films (Fig. 2a) exhibit two diffraction peaks with (111) and (511) orientations for the typical CdTe with cubic zinc blende structure.

The peak for the (111) plane at $\sim 2\theta = 23.7°$ in all as-deposited films

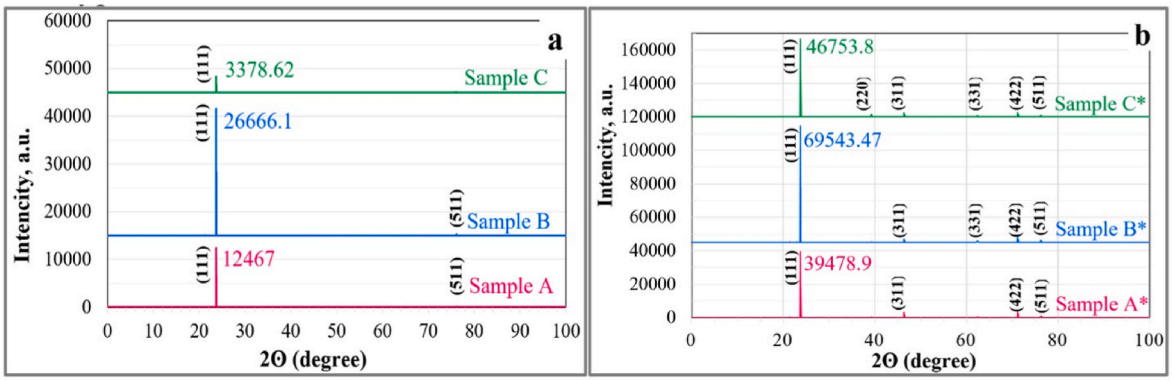

Fig. 2. XRD diffractogram of deposited (a) and annealed (b) CdTe samples.

has significantly higher intensities compared to all other planes that have negligibly small intensities. These results suggest that all films have preferentially grown with an (111) orientation, which is perpendicular to the substrate. The amorphous nature of the glass substrate cannot influence such a preferential grain orientation in the film. After annealing, the films possess the typical polycrystalline nature of cubic CdTe (ICDD, PDF# 00-015-0770) structure, exhibiting (220), (311), (331), (422), and (511) plane orientations along with the intense (111) reflection (Fig. 2b). Such an increase in the number of plane orientations other than (111) indicates refinement of the structure through the recrystallization process at the annealing step. Fig. 2b also suggests that the films prepared in the presence of CdCl2 have improved the crystallinity after annealing as the intensities of (111) reflection are significantly higher for the samples B* and C* compared to sample A*. For samples A, B and C the (111) peak intensity numerical values were 12,467, 26,666 and 3378 respectively. After annealing, the (111) peak intensity numerical values of samples A*, B* and C* became 39,479, 69,543 and 46,753, respectively.

Table 1 summarizes peak position, full-width of half-maximum (FWHM, β) as well as crystallographic parameters, such as lattice constant ($a = d\sqrt{h^2 + k^2 + l^2}$), interplanar spacing (2dsinθ = λ), the mean size of the crystalline domains ($\tau = \frac{0.9\bullet\lambda}{\beta\bullet\cos(\theta)}$), dislocation density (δ = 1/τ2), number of crystallites per unit area (N = t/τ3) and internal strain (ε = $\boldsymbol{\beta}\bullet\cos(\boldsymbol{\theta})/4$), where λ is the wavelength of the X-ray used (λ = 1.5405 Å), β is the full-width at half-maximum (FWHM) of the peak and (θ) is the Bragg's angle and t is the thickness.

These parameters were calculated from the characteristics of the peak for the (111) plane orientations for both as-deposited and annealed CdTe films according to methods reported elsewhere [25,32,36]. The results show that the lattice constant (*a*) of sample A is 0.6491 nm. The lattice constants of the samples B and C are 0.6497 nm and 0.6502 nm, respectively. After annealing, the lattice constant of all samples slightly decreased to ~0.6484 nm. The d-spacing of all as-grown films varies in the range 0.3748–0.3754 nm. Annealing leads to a certain decrease in the d-spacing to the value ~0.3744 for all films.

The size of the crystalline domains (τ) calculated by the Scherrer formula for all three as-deposited samples is approximately 87 nm, while after annealing of the samples, the τ values increase. This increase is more significant for $CdCl_2$ containing samples (from 87 nm to ~174 nm) compared to pure CdTe sample (from 87 nm to 130 nm). The annealing reduces the dislocation density δ of films from 1.33·1010 to 0.59·1010 cm-2 for sample A* and from 1.33·1010 to 0.33·1010 cm-2 for samples B* and C*. The number of crystallites per unit area (N) is found to be in the range $60.2{\cdot}10^{10}$–$62.53{\cdot}10^{10}$ cm^{-2} for as-deposited samples. This parameter also decreases ($7.52{\cdot}10^{10}$–$18.30{\cdot}10^{10}$ cm^{-2}) for thermally annealed samples due to an increase in the grain size. The values of internal microstrain in the samples change almost twice after annealing. All these calculated results suggest that the incorporation of $CdCl_2$ in the CdTe film bulk of significantly improves the crystallinity of the CdTe films. Accordingly, XRD data has demonstrated that thermal annealing causes the following changes: a) a practically complete match in the lattice parameter of film with the conventional value; b) a sharp increase in the intensity of the diffraction peak; and c) a growth in grain sizes and a decline in the dislocation density, micro-strain and number of crystallites per unit area.

3.2. Surface morphology of films

AFM analysis was performed to investigate the surface morphology of all six samples. Three- and two-dimensional AFM visualizations of samples are shown in Fig. 3a and b. These images show bright protrusions and dark valleys. Information about the maximum and minimum surface roughness can be obtained from the 2D image areas (Fig. 3b). Sample A exhibits the highest surface roughness (±65 nm). The increase in the fraction of $CdCl_2$ during deposition results in some decrease in the surface roughness. For example, samples B and C exhibit surface roughness of ~±50 and ~±40 nm, respectively. Thermal annealing within measurement accuracy does not change the roughness (Fig. 3b).

Based on grain size distribution histograms, it is possible to estimate, the average range of grain size variation. The average range of grain size variation was determined from the half maximum of the grain count distribution (Fig. 3c). The determined grain size range for samples A, B, C, are 300–650 nm, 250–550 nm, 350–800 nm, and for samples A*, B*,

Table 1
The results of some crystallographic parameters extracted from XRD patterns of CdTe films.

Sample	Peak position (2θ), °	FWHM (β), °	Interplanar spacing (d), nm	Lattice constant (a), nm	Size of the crystalline domains (τ), nm	Dislocation density ($\delta{\cdot}10^{10}$), cm^{-2}	Number of crystallites ($N{\cdot}10^{10}$), cm^{-2}	Internal strain, ($\varepsilon{\cdot}10^{-4}$)
A	23.7234	0.0936	0.3748	0.6491	86.76	1.33	61.78	3.99
B	23.7021	0.0936	0.3751	0.6497	86.76	1.33	60.20	4.00
C	23.6825	0.0936	0.3754	0.6502	86.76	1.33	62.53	4.00
A*	23.7481	0.0624	0.3744	0.6484	130.15	0.59	18.30	2.66
B*	23.7463	0.0468	0.3744	0.6485	173.53	0.33	7.52	2.00
C*	23.7507	0.0468	0.3743	0.6484	173.54	0.33	7.81	2.00

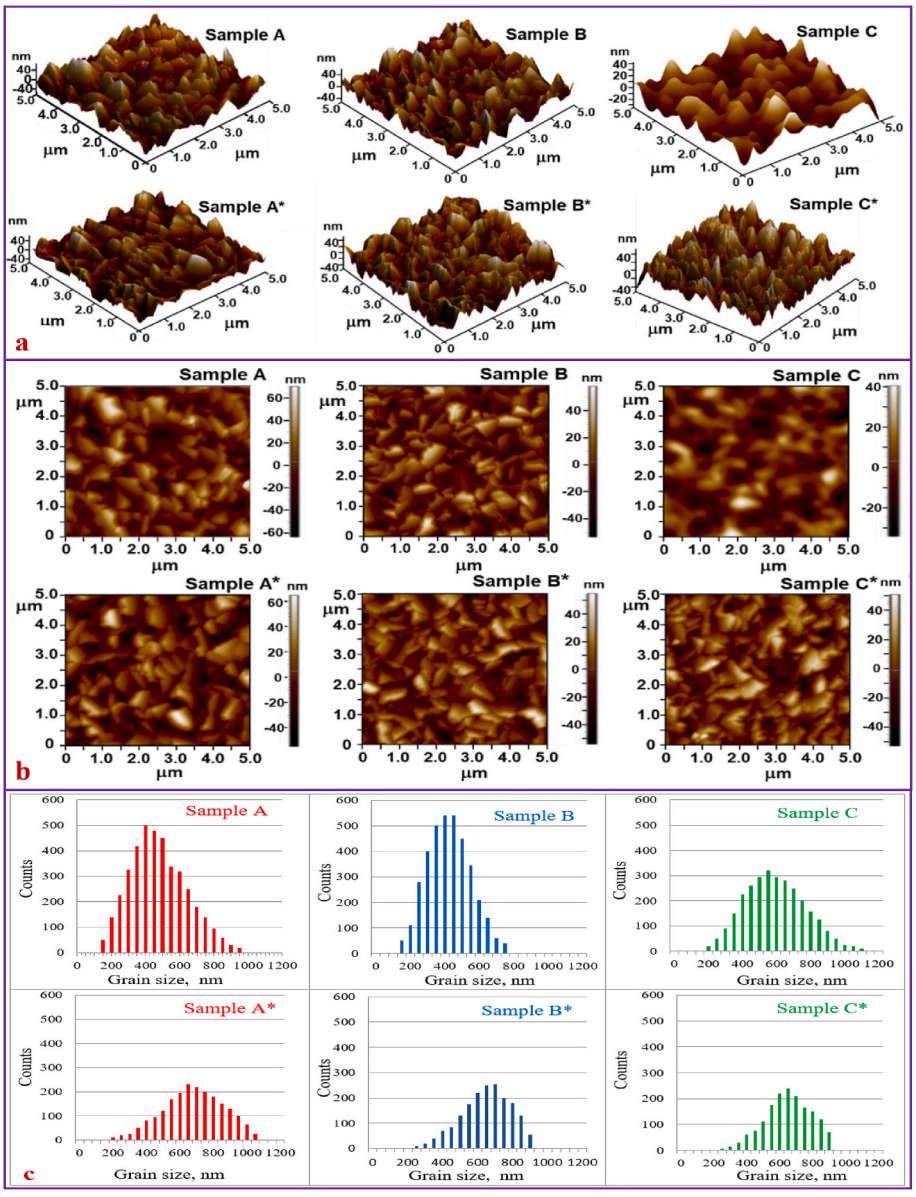

Fig. 3. AFM three-dimensional (a) and two-dimensional (b) view and distributions of the grain size (c) of the as-deposited and annealed sample determined from AFM images.

C* 500–900 nm, 500–850 nm, 550–850 nm respectively.

According to these findings, the average range of grain size variation for CdTe films while they are deposited is essentially between 0.3 and 0.8 μm, and following thermal annealing, it rises to values between 0.5 and 0.9 μm.

We also used SEM imaging to investigate the surface morphology of annealed samples. Fig. 4 shows the surface morphology of the samples. Samples A* and B* have irregular granular structures with relatively small grains and uniform surface coverage of grains without any cracks or voids. The grains in the sample C* are somewhat larger, suggesting that increasing the concentration of $CdCl_2$ during deposition helps to obtain coarse-grained material after annealing.

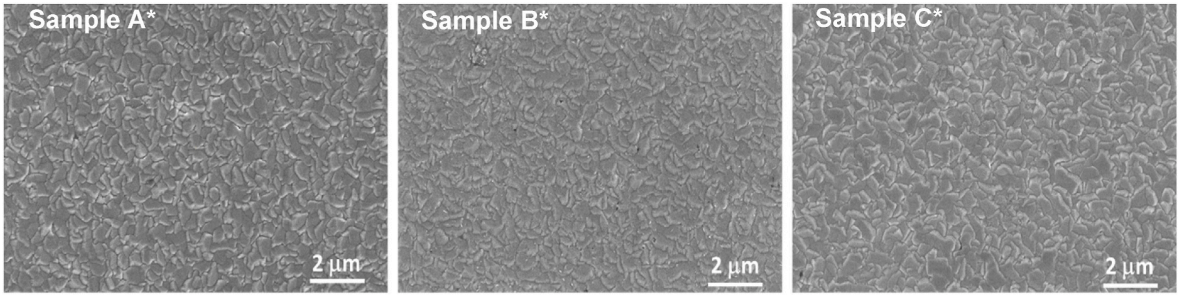

Fig. 4. SEM images of annealed CdTe samples.

3.3. Internal morphology and the structure of films

The cross-sectional SEM images of the annealed samples (Fig. 5a) show that all the films have a thickness of approximately 4 μm with a compact morphology, free of voids or other imperfections.

Cross-sectional images of all three samples exhibit a few twin boundaries or intrinsic/extrinsic stacking faults that go across CdTe grains and terminate at grain boundaries or interfaces (marked by arrows in Fig. 5a). These types of features are commonly observed in previous works [55,56] and sometimes considered stacking fault regions with CdTe wurtzite structure. We should note that the quantity of such stacking faults in all those samples is significantly lower compared with the materials prepared by the CSS process [14]. Due to the much higher deposition temperatures (500–600 °C) in the CSS small nuclei tend to re-evaporate, and only more significant nuclei with larger sizes from a critical radius are grown rapidly in uncontrolled and non-equilibrium manner. In contrast, our samples contain a significant amount of well-defined three-dimensional vertical columnar CdTe grains without any visible faults. The width of these columnar grains is about 1000–2000 nm. This result suggests that the low-temperature DVTE method used in this work provides controlled and equilibrium growth of high-quality pore-free films with relatively larger crystalline grains.

The reason behind such a distinctive growth feature can be related to the mechanism of nucleation, grain growth, and the coalescence of crystals at the DVTE method. The low-temperature nature of this deposition process allows the formation of small stable nuclei that do not re-evaporate. The population density of small nuclei is relatively high. Therefore, many small nuclei have a much higher probability of successfully growing into grains during the process. The steady supply of vaporizing CdTe ensures a constant atomic flux of Cd and Te to maintain the stable growth of columnar CdTe grains with (111) preferential crystallographic orientation (Fig. 2a).

We can assume that in situ evaporation of $CdCl_2$ provides uniform distribution of chlorine in the CdTe lattices during the deposition stage. The presence of chlorine dopant plays a significant role in structural and morphological refinements during the post-deposition annealing stage. We can suggest that highly mobile chlorine ions diffuse to the grain boundaries and thus facilitate the recrystallization processes, forming large and well-defined grains.

To elucidate the internal structure of grains, focused ion beam cross-sections were prepared for TEM analysis across the CdTe layer. The bright-field TEM images of the CdTe layers are shown in Fig. 5b. The white circles within the dark grains show the region of interest for the selected area diffraction (SAD) pattern. The indexed SAD patterns for

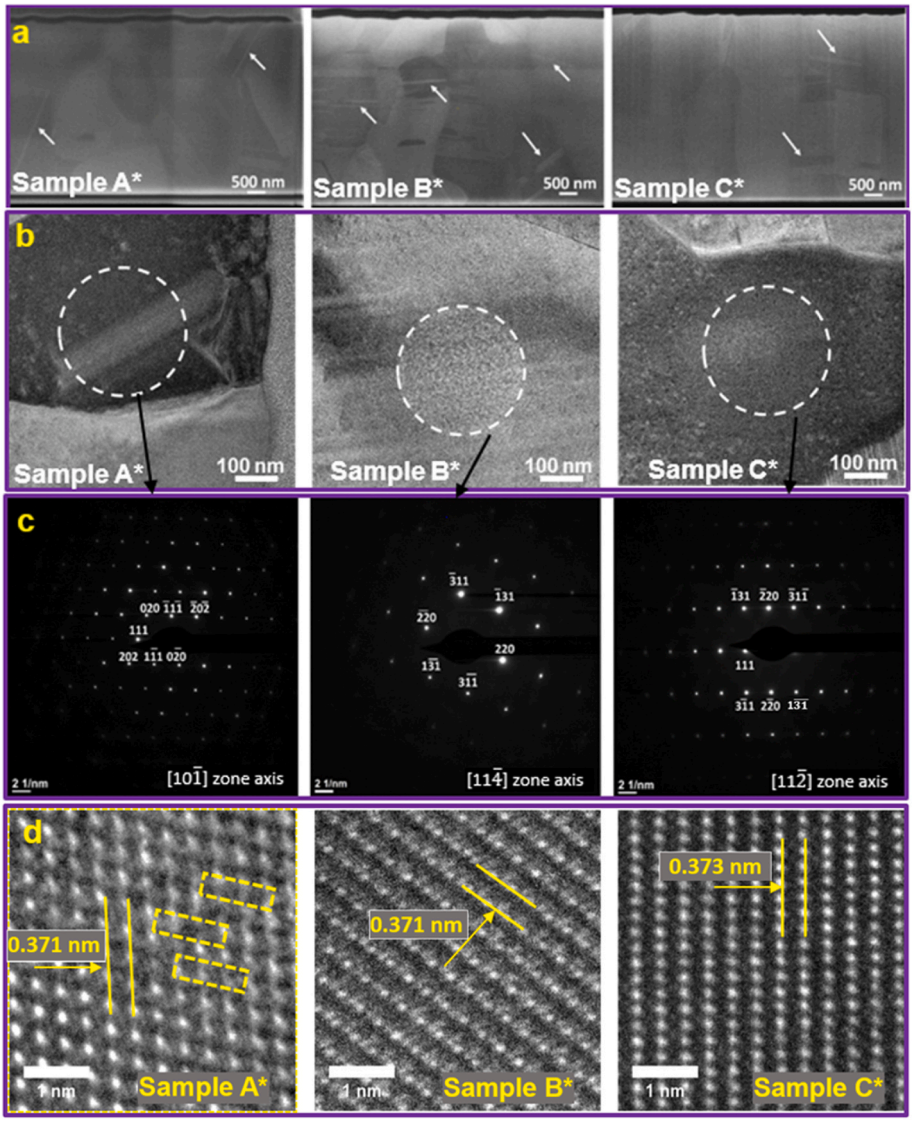

Fig. 5. Cross-sectional SEM images (a), bright-field TEM images (b), SAD patterns (c) of associated are-as, and high-resolution TEM images (d) for the annealed samples. Twin boundaries or intrin-sic/extrinsic stacking faults are marked by arrows on panel 5a.

sample A* shown in Fig. 5c are consistent with the CdTe zinc blende structure with a grain aligned along the [101] zone axis. The SAD pattern from a grain (sample B*) is oriented along the [114] zone axis and is also indexed as the cubic zinc blende structure of CdTe. The grain from the sample C* also exhibits cubic structure and is oriented along the [112] axis.

High-resolution TEM images of the selected grains are shown in Fig. 5d. Viewed along the [110] orientation of grains, the crystal can be seen as columns composed of pairs of Te and Cd atoms. A grain of the sample A* exhibits several intra-grain Shockley partial dislocations marked with yellow rectangles. The measured d-spacing for the [111] orientation is 0.371 nm. High-resolution TEM images of B* and C* samples grains do not exhibit visible intra-grain dislocations. The d-spacing for the [111] orientation is 0.371 and 0.373 nm.

4. Conclusion

This study discusses the impact of discrete vacuum thermal evaporation (DVTE)-produced CdTe thin films after thermal annealing and $CdCl_2$ treatment. For the first time, $CdCl_2$ was added to a CdTe film during this study using synchronous DVTE of $CdCl_2$ and CdTe rather than diffusion through the surface after its deposition.

According to XRD measurements, all CdTe thin films feature a cubic zinc blende structure with a predominately high intensity sharp peak, which is assigned to the (111) crystallographic orientation plane. It is found that introducing $CdCl_2$ into the CdTe film bulk during its deposition results in a crystal structure that is more ideal.

Following thermal annealing, the typical range of grain size variation for deposited CdTe films grew from 0.3 to 0.8 μm to values between 0.5 and 0.9 m, according to the AFM investigation.

Cross-sectional SEM images showed that CdTe films contain a significant amount of well-defined three-dimensional vertical columnar CdTe grains without any visible faults. The width of these columnar grains is about 1000–2000 nm. The reason behind such a distinctive growth feature can be related to the mechanism of grain growth at the DVTE method. The steady supply of vaporizing CdTe ensures a constant atomic flux of Cd and Te to maintain the stable growth of columnar CdTe grains.

In situ evaporation of $CdCl_2$ provides uniform distribution of chlorine in the CdTe lattices during the deposition stage. The presence of chlorine dopant plays a significant role in structural and morphological refinements during the post-deposition annealing stage. High-resolution TEM images showed that CdTe films doped with CdCl2 do not exhibit visible intra-grain dislocations.

XRD, AFM, FIB, SEM, and TEM findings have demonstrated that the DVTE approach used in this work provides controlled and equilibrium growth of high-quality CdTe films with relatively larger crystalline grains, which can be used productively to create high-efficiency solar cells.

CRediT authorship contribution statement

V.A. Gevorgyan: Writing – review & editing, Writing – original draft, Supervision, Project administration, Methodology, Investigation, Funding acquisition, Conceptualization. **N.R. Mangasaryan:** Writing – review & editing, Methodology, Investigation, Funding acquisition, Formal analysis, Data curation. **V.F. Gremenok:** Writing – original draft, Visualization, Validation, Software, Resources, Project administration, Formal analysis. **M.S. Tivanov:** Writing – review & editing, Writing – original draft, Visualization, Validation, Software, Resources. **Preeti Thakur:** Software, Methodology, Formal analysis. **Atul Thakur:** Writing – review & editing, Visualization, Formal analysis. **S.V. Trukhanov:** Writing – review & editing, Writing – original draft, Visualization. **T.I. Zubar:** Writing – original draft, Visualization. **M.I. Sayyed:** Writing – review & editing, Investigation. **D.I. Tishkevich:** Writing – review & editing, Writing – original draft, Investigation. **A.V. Trukhanov:** Writing – review & editing, Writing – original draft, Supervision, Investigation.

Declaration of competing interest

The authors declare that they have no known competing financial interests or personal relationships that could have appeared to influence the work reported in this paper.

Dr. Daria Tishkevich May 16, 2023.

Data availability

Data will be made available on request.

Acknowledgment

The Ministry of Education and Science of the Russian Federation is appreciated by the authors for supporting the research efforts of the RAU.

References

[1] Y. Zhao, M. Boccard, S. Liu, J. Becker, X.H. Zhao, C.M. Campbell, E. Suarez, M. B. Lassise, Z. Holman, Y.H. Zhang, Monocrystalline CdTe solar cells with open-circuit voltage over 1 v and efficiency of 17, Nat. Energy 1 (2016) 1–7, https://doi.org/10.1038/nenergy.2016.67.

[2] O. Toma, L. Ion, M. Girtan, S. Antohe, Optical, morphological and electrical studies of thermally vacuum evaporated CdTe thin films for photovoltaic applications, Sol. Energy 108 (2014) 51–60, https://doi.org/10.1016/j.solener.2014.06.031.

[3] A. Romeo, E. Artegiani, D. Menossi, Low substrate temperature CdTe solar cells: a review, Sol. Energy 175 (2018) 9–15, https://doi.org/10.1016/j.solener.2018.02.038.

[4] D.I. Tishkevich, A.I. Vorobjova, A.V. Trukhanov, Thermal stability of nanocrystalline nickel electrodeposited into porous alumina, Solid State Phenom 299 (2020) 281–286. https://doi.org/10.4028/www.scientific.net/SSP.299.281.

[5] M. Gloeckler, I. Sankin, Z. Zhao, CdTe solar cells at the threshold to 20% efficiency, J. Photovoltaics 3 (2013) 1389–1393, https://doi.org/10.1109/JPHOTOV.2013.2278661.

[6] J.M. Kurley, M.G. Panthani, R.W. Crisp, S.U. Nanayakkara, G.F. Pach, M.O. Reese, M.H. Hudson, D.S. Dolzhnikov, V. Tanygin, J.M. Luther, D.V. Talapin, Transparent ohmic contacts for solution-processed, ultrathin CdTe solar cells, ACS Energy Lett. 2 (2017) 270–278, https://doi.org/10.1021/acsenergylett.6b00587.

[7] X. Mathew, N.R. Mathews, P.J. Sebastian, C. Osvaldo Flores, Deep levels in the band gap of CdTe films electrodeposited from an acidic bath - PICTS analysis, Sol. Energy Mater. Sol. Cells 81 (2004) 397–405, https://doi.org/10.1016/j.solmat.2003.11.015.

[8] I. Ban, M. Kristl, V. Danč, A. Danč, M. Drofenik, Preparation of cadmium telluride nanoparticles from aqueous solutions by sonochemical method, Mater. Lett. 67 (2012) 56–59, https://doi.org/10.1016/j.matlet.2011.09.001.

[9] B. Ghosh, S. Hussain, D. Ghosh, R. Bhar, A.K. Pal, Studies on CdTe films deposited by pulsed laser deposition technique, Phys. B Condens. Matter 407 (2012) 4214–4220, https://doi.org/10.1016/j.physb.2012.07.006.

[10] A. Vorobjova, D. Tishkevich, D. Shimanovich, T. Zubar, K. Astapovich, A. Kozlovskiy, M. Zdorovets, A. Zhaludkevich, D. Lyakhov, D. Michels, D. Vinnik, V. Fedosyuk, A. Trukhanov, The influence of the synthesis conditions on the magnetic behaviour of the densely packed arrays of Ni nanowires in porous anodic alumina membranes, RSC Adv 11 (2021) 3952, https://doi.org/10.1039/d0ra07529a.

[11] T.L. Chu, S.S. Chu, C. Ferekides, J. Britt, C.Q. Wu, Thin-film junctions of cadmium telluride by metalorganic chemical vapor deposition, J. Appl. Phys. 71 (1992) 3870–3876, https://doi.org/10.1063/1.350852.

[12] A. Bosio, S. Pasini, N. Romeo, The history of photovoltaics with emphasis on CdTe solar cells and modules, Coatings 10 (2020), https://doi.org/10.3390/coatings10040344.

[13] D. Suthar, S. Chuhadiya, R. Sharma, Himanshu, M.S. Dhaka, An overview on the role of ZnTe as an efficient interface in CdTe thin film solar cells: a review, Adv. Mater. 22 (2022), https://doi.org/10.1039/D2MA00817C.

[14] C. Li, J. Poplawsky, Y. Yan, S.J. Pennycook, Understanding individual defects in CdTe thin-film solar cells via STEM: from atomic structure to electrical activity, Mater. Sci. Semicond. Process. 65 (2017) 64–76, https://doi.org/10.1016/j.mssp.2016.06.017.

[15] I.M. Dharmadasa, A. P Samantilleke, N.B. Chaure, J. Young, New ways of developing glass/conducting glass/CdS/CdTe/metal thin-film solar cells based on a new model, Semicond. Sci. Technol. 17 (2002) 1238–1248, https://doi.org/10.1088/0268-1242/17/12/306.

[16] G. Khrypunov, A. Romeo, F. Kurdesau, D.L. Bätzner, H. Zogg, A.N. Tiwari, Recent developments in evaporated CdTe solar cells, Sol. Energy Mater. Sol. Cells 90 (2006) 664–677, https://doi.org/10.1016/j.solmat.2005.04.003.

[17] D.A. Lamb, C.I. Underwood, V. Barrioz, R. Gwilliam, J. Hall, M.A. Baker, S.J. C. Irvine, Proton irradiation of CdTe thin film photovoltaics deposited on cerium-doped space glass, Prog. Photovoltaics Res. Appl. 25 (2017) 1059–1067, https://doi.org/10.1002/pip.2923.
[18] N. Romeo, A. Bosio, V. Canevari, A. Podestà, Recent progress on CdTe/CdS thin film solar cells, Sol. Energy 77 (2004) 795–801, https://doi.org/10.1016/j.solener.2004.07.011.
[19] R. Luo, B. Liu, X. Yang, Z. Bao, B. Li, J. Zhang, W. Li, L. Wu, L. Feng, The large-area CdTe thin film for CdS/CdTe solar cell prepared by physical vapor deposition in medium pressure, Appl. Surf. Sci. 360 (2016) 744–748, https://doi.org/10.1016/j.apsusc.2015.11.058.
[20] A.L. Kozlovskiy, I.E. Kenzhina, M.V. Zdorovets, M. Saiymova, D.I. Tishkevich, S. V. Trukhanov, A.V. Trukhanov, Synthesis, phase composition and structural and conductive properties of ferroelectric microparticles based on ATiOx (A = Ba, Ca, Sr), Ceram. Int. 45 (2019) 17236–17242, https://doi.org/10.1016/j.ceramint.2019.05.279.
[21] J.A. Ríos-González, R. Mis-Fernández, E. Camacho-Espinosa, I. Riech, E. Menéndez- M.A. Proupin, Flores, W. Orellana, J.L. Peña, Inducing a level inside of CdTe bandgap doping with Sn using a co-sublimation technique by CSS, Mater. Sci. Semicond. Process. 107 (2020) 17–19, https://doi.org/10.1016/j.mssp.2019.104836.
[22] K.S. Rahman, M.N. Harif, H.N. Rosly, M.I. bin Kamaruzzaman, Md Akhtaruzzaman, M. Alghoul, H. Misran, N. Amin, Influence of deposition time in CdTe thin film properties grown by Close-Spaced Sublimation (CSS) for photovoltaic application, Results Phys. 14 (2019), 102371, https://doi.org/10.1016/j.rinp.2019.102371.
[23] N. Spalatu, J. Hiie, V. Valdna, M. Caraman, N. Maticiuc, V. Mikli, T. Potlog, M. Krunks, V. Lughi, Properties of the CdCl2 air-annealed CSS CdTe thin films, Energy Proc. 44 (2014) 85–95, https://doi.org/10.1016/j.egypro.2013.12.013.
[24] Z. Bao, X. Yang, B. Li, R. Luo, B. Liu, P. Tang, J. Zhang, L. Wu, W. Li, L. Feng, The study of CdSe thin film prepared by pulsed laser deposition for CdSe/CdTe solar cell, J. Mater. Sci. Mater. Electron. 27 (2016) 7233–7239, https://doi.org/10.1007/s10854-016-4689-9.
[25] D.G. Diso, F. Fauzi, O.K. Echendu, O.I. Olusola, I.M. Dharmadasa, Optimisation of CdTe electrodeposition voltage for development of CdS/CdTe solar cells, J. Mater. Sci. Mater. Electron. 27 (2016) 12464–12472, https://doi.org/10.1007/s10854-016-4844-3.
[26] B.M. Basol, Electrodeposited CdTe and HgCdTe solar cells, Sol. Cell. 23 (1988) 69–88, https://doi.org/10.1016/0379-6787(88)90008-7.
[27] S. Sohal, M. Edirisooriya, T. Myers, M. Holtz, Investigation of cadmium telluride grown by molecular-beam epitaxy using micro-Raman spectroscopy below and above the laser damage threshold, J. Vac. Sci. Technol. B 36 (2018), 052905, https://doi.org/10.1116/1.5048526.
[28] V.S. Evstigneev, A.V. Chilyasov, A.N. Moiseev, M.V. Kostunin, Incorporation and activation of arsenic in single-crystal CdTe layers grown by metalorganic chemical vapor deposition, Thin Solid Films 689 (2019), 137514, https://doi.org/10.1016/j.tsf.2019.137514.
[29] A.D. Compaan, A. Gupta, S. Lee, S. Wang, J. Drayton, High efficiency, magnetron sputtered CdS/CdTe solar cells, Sol. Energy 77 (2004) 815–822, https://doi.org/10.1016/j.solener.2004.06.013.
[30] N.R. Paudel, K.A. Wieland, A.D. Compaan, Ultrathin CdS/CdTe solar cells by sputtering, Sol. Energy Mater. Sol. Cells 105 (2012) 109–112, https://doi.org/10.1016/j.solmat.2012.05.035.
[31] P.K.K. Kumarasinghe, A. Dissanayake, B.M.K. Pemasiri, B.S. Dassanayake, Effect of post deposition heat treatment on mi-crostructure parameters, optical constants and composition of thermally evaporated CdTe thin films, Mater. Sci. Semicond. Process. 58 (2017) 51–60, https://doi.org/10.1016/j.mssp.2016.11.028.
[32] L.G. Daza, R. Castro-Rodríguez, E.A. Martín-Tovar, A. Iribarren, CdTe films grown using a rotating sublimate vapor effu-sion source in glancing angle deposition mode, Mater. Sci. Semicond. Process. 59 (2017) 23–28, https://doi.org/10.1016/j.mssp.2016.09.042.
[33] E.R. Shaaban, I.S. Yahia, N. Afify, G.F. Salem, W. Dobrowolski, Structural and the optical dispersion parameters of nano-CdTe thin film/flexible substrate, Mater. Sci. Semicond. Process. 19 (2014) 107–113, https://doi.org/10.1016/j.mssp.2013.12.013.
[34] N.A. Bakr, Characterization of a CdZnTe/CdTe heterostructure system prepared by Zn diffusion into a CdTe thin film, J. Cryst. Growth 235 (2002) 217–223, https://doi.org/10.1016/S0022-0248(01)01732-8.
[35] H.D. Yang, C.Y. Zhang, Y. Wang, L. Chen, B.R. Peng, H. Liu, Effect of substrate temperature on structure and optical properties of CdTe films, J. Synth. Cryst. 46 (2017) 2102–2106. 10.18052/www.scipress.com/ilcpa.27.47.
[36] D.I. Tishkevich, T.I. Zubar, A.L. Zhaludkevich, I.U. Razanau, T.N. Vershinina, A. A. Bondaruk, E.K. Zheleznova, M. Dong, M.Y. Hanfi, M.I. Sayyed, M.V. Silibin, S. V. Trukhanov, A.V. Trukhanov, Isostatic hot pressed W–Cu composites with nanosized grain boundaries: microstructure, structure and radiation shielding efficiency against gamma rays, Nanomaterials 12 (2022) 1642, https://doi.org/10.3390/nano12101642.
[37] A. Salavei, I. Rimmaudo, F. Piccinelli, A. Romeo, Influence of CdTe thickness on structural and electrical properties of CdTe/CdS solar cells, Thin Solid Films 535 (2013) 257–260, https://doi.org/10.1016/j.tsf.2012.11.121.
[38] S. Kumari, D. Suthar, Himanshu, N. Kumari, M.S. Dhaka. Understanding Grain Growth Mechanism in Vacuum Evaporated CdTe Thin Films by Different Halide Treatments: An Evolution of Ion Size Impact on Physical Properties for Solar Cell Applications. Comments Inorg.. https://doi.org/10.1080/02603594.2022.2142938.
[39] S. Chander, M.S. Dhaka, Preparation and physical characterization of CdTe thin films deposited by vacuum evaporation for photovoltaic applications, Adv. Mater. Lett. 6 (10) (2015) 907–912, https://doi.org/10.5185/amlett.2015.5926.
[40] J. Lee, Effects of heat treatment of vacuum evaporated CdCl2 layer on the properties of CdS/CdTe solar cells, Curr. Appl. Phys. 11 (2011) S103–S108, https://doi.org/10.1016/j.cap.2010.11.099.
[41] S. Chander, M.S. Dhaka, Time evolution to CdCl2 treatment on Cd-based solar cell devices fabricated by vapor evapora-tion, Sol. Energy 150 (2017) 577–583, https://doi.org/10.1016/j.solener.2017.05.013.
[42] S. Chander, M.S. Dhaka, $CdCl_2$ treatment concentration evolution of physical properties correlation with surface morphology of CdTe thin films for solar cells, Mater. Res. Bull. 97 (2018) 128–135, https://doi.org/10.1016/j.materresbull.2017.08.038.
[43] L. Patel, Himanshu, S. Chander, M.D. Kannan, M.S. Dhaka, Impact of chloride treatment on the physical properties of polycrystalline thin CdTe films for solar cell applications, Phys. Lett. 383 (15) (2019) 1778–1781, https://doi.org/10.1016/j.physleta.2019.03.001.
[44] N. Amin, M. Rezaul Karim, Z.A. Alothman, Impact of $CdCl_2$ treatment in CdTe thin film grown on ultra-thin glass substrate via close spaced sublimation, Crystals 11 (4) (2021) 390, https://doi.org/10.3390/cryst11040390.
[45] S. Chander, S.K. Tripathi, Advancement in CdMnTe-based photovoltaic cells: grain growth, deep states and device efficiency assessment with chlorine treatment, Sol. Energy 250 (2023) 91–96, https://doi.org/10.1016/j.solener.2022.12.033.
[46] O. Vigil-Gaín, A. Arias-Carbajal, R. Mendoza-Pérez, G. Santana-Rodríguez, J. Sastre-Hernández, J.C. Alonso, E. More-no-García, G. Contreras-Puente, A. Morales-Acevedo, Improving the efficiency of CdS/CdTe solar cells by varying the thiourea/CdCl2 ratio in the CdS chemical bath, Semicond. Sci. Technol. 20 (2005) 819–822, https://doi.org/10.1088/0268-1242/20/8/032.
[47] V. Bilgin, S. Kose, F. Atay, I. Akyuz, The effect of substrate temperature on the structural and some physical properties of ultrasonically sprayed CdS films, Mater. Chem. Phys. 94 (2005) 103–108, https://doi.org/10.1016/j.matchemphys.2005.04.028.
[48] A. López-Sánchez, I. Rimmaudo, R. Mis-ernández, E. Camacho-Espinosa, J.L. Peña, Effect of the air humidity on the chlorine treatment for CdTe thin films solar cells, Sol. Energy 239 (2022) 129–138, https://doi.org/10.1016/j.solener.2022.04.063.
[49] V.A. Gevorkyan, A.E. Reymers, M.N. Nersesyan, M.A. Arzakantsyan, Characterization of Cu2O thin films prepared by evaporation of CuO powder, J. Phys. Conf. Ser. 350 (2012), https://doi.org/10.1088/1742-6596/350/1/012027, 0–6.
[50] M. Hemanadhan, C. Bapanayya, S.C. Agarwal, Simple flash evaporator for making thin films of compounds, J. Vac. Sci. Technol. A 28 (2010) 625–626, https://doi.org/10.1116/1.3443567.
[51] V.A. Gevorgyan, L.A. Hakhoyan, N.R. Mangasaryan, P.P. Gladyshev, Substrate temperature and annealing effects on the structural and optical properties of nano-CdS films deposited by vacuum flash evaporation technique, Chalcogenide Lett. 13 (2016) 331–338, https://doi.org/10.15761/fnn.1000114.
[52] F.M.T. Enam, K.S. Rahman, M.I. Kamaruzzaman, K. Sobayel, M. Aktharuzzaman, N. Amin, An investigation on structural and electrical properties of close-spaced sublimation grown CdTe thin films in different growth conditions, Chalcogenide Lett. 14 (2016) 125–131.
[53] K. Manukyan, C. Fasano, A. Majumdar, G.F. Peaslee, M. Raddell, E. Stech, M. Wiescher, Surface manipulation techniques of Roman denarii, Appl. Surf. Sci. 493 (2019) 818–828, https://doi.org/10.1016/j.apsusc.2019.06.296.
[54] P. Sapkota, A. Aprahamian, K.Y. Chan, B. Frentz, K.T. Macon, D. Robertson, K. Manukyan, Irradiation-induced reactions at the CeO2/SiO2/Si interface, J. Chem. Phys. 152 (2020), 104704, https://doi.org/10.1063/1.5142619.
[55] J. Luria, Y. Kutes, A. Moore, L. Zhang, E.A. Stach, B.D. Huey, Charge transport in CdTe solar cells revealed by conductive tomographic atomic force microscopy, Nat. Energy 1 (2016) 1–6, https://doi.org/10.1038/nenergy.2016.150.
[56] J.D. Poplawsky, W. Guo, N. Paudel, A. Ng, K. More, D. Leonard, Y. Yan, Structural and compositional dependence of the CdTex Se1-x alloy layer photoactivity in CdTe-based solar cells, Nat. Commun. 7 (2016) 1–10, https://doi.org/10.1038/ncomms12537.